ELSEVIER

Nuclear Instruments and Methods in Physics Research A 480 (2002) 440–447

NUCLEAR INSTRUMENTS & METHODS IN PHYSICS RESEARCH Section A

www.elsevier.com/locate/nima

Measurements of the response functions of an NE213 organic liquid scintillator to neutrons up to 800 MeV

M. Sasaki[a], N. Nakao[b], T. Nakamura[a,*], T. Shibata[b], A. Fukumura[c]

[a] *Department of Quantum Science and Energy Engineering, Tohoku University, Aza-Aoba 01, Aramaki, Aoba-ku, Sendai-Shi 980-8579, Japan*

[b] *High Energy Accelerator Research Organization(KEK), Oho 1-1, Tsukuba, Ibaraki 305-0801, Japan*

[c] *National Institute of Radiological Sciences(NIRS), Anagawa 4-9-1, Inageku, Chiba-shi 263-8555, Japan*

Received 30 October 2000; received in revised form 6 March 2001; accepted 24 March 2001

Abstract

The neutron response functions of 12.7 cm diameter by 12.7 cm long NE213 organic liquid scintillator have been measured in the energy range from 50 to 800 MeV at the Heavy-Ion Medical Accelerator in Chiba (HIMAC). Neutrons were generated by the 800 MeV/nucleon Si ion and 400 MeV/nucleon C ion bombardment on a thick carbon target. Neutron energy was determined by the time-of-flight method with using the beam pick-up scintillator. The maximum light outputs were gradually increased with increasing incident neutron energy and the variation of the response functions have been observed up to 800 MeV. The experimental results show good agreement with other experimental results and the calculated values for incident neutron energy below about 200 MeV.

PACS: 29.30.Hs; 29.40.Mc

Keywords: Response functions; Neutron spectrometry; NE213 Organic liquid scintillator; Time-of-flight method; Cecil code

1. Introduction

An NE213 organic liquid scintillator coupled with a photo-multiplier is widely used for high energy neutron spectrometry with the time-of-flight method and the unfolding method because of good quality of neutron and photon discrimination. The physical characteristics of the NE213 scintillator, such as response functions, detection efficiencies and light output mechanisms, have been studied and are well known in detail for neutrons below 20 MeV nowadays.

With regard to the response functions for neutrons above 20 MeV, several experiments [1–4] and Monte Carlo simulations [5–7] have been done. Nakao et al. measured the response functions in the energy range up to 135 MeV [4] using the Li(p,n) quasi-monoenergetic and white neutron sources developed at the cyclotron facilities in Japan. Recently, they extended the response functions up to 206 MeV [8] using the

*Corresponding author. Tel.: +81-22-217-7805; fax: +81-22-217-7809.

E-mail address: nakamura@cyric.tohoku.ac.jp (T. Nakamura).

0168-9002/02/$ - see front matter
PII: S0168-9002(01)00948-2

same quasi-monoenergetic neutron fields [9]. By comparing the results with the Monte Carlo calculation, they pointed out some discrepancy between the experiments and the calculations. Sailor and Byrd [10] calculated the response functions of BC501A and NE213 for neutrons of energy up to 492 MeV. About the detection efficiency, Borne et al. measured the efficiency of 12.7 cm diameter by 15 cm long NE213 scintillator up to 800 MeV using the Be(d,n) monoenergetic neutron field [11]. Although there are some reports about response functions for high energy neutrons above 100 MeV, the experimental approaches are very scarce and especially, there is no published response function beyond 200 MeV.

To obtain neutron energy spectra, the unfolding codes, such as FERDO [12], FERDO-U [13] and FORIST [14], are commonly used with measured and calculated response functions. This method has the advantage that the measuring circuit is comparatively simple as there is no need for the time information and it can be used to measure not only neutrons generated from the target directly [15] but also neutrons penetrated through a matter [16]. However, this method has mainly been used for neutron measurement of energy up to several ten MeV and there has been no application to measure neutrons higher than 100 MeV with the unfolding procedure because of a lack of response functions to high energy neutrons with good accuracy.

Here in this study, we measured the response functions of 12.7 cm diam. by 12.7 cm long NE213 scintillator for neutrons in the energy range from 50 to 800 MeV at the Heavy-Ion Medical Accelerator in Chiba (HIMAC) of National Institute of Radiological Sciences (NIRS), Japan. Neutrons were generated by bombardment of high energy heavy ions on a thick (stopping length) target. The source neutron energy was determined by the time-of-flight method and the absolute neutron yields emitted at different angles from the target have already been measured by Kurosawa et al. [17–19] for various combinations of projectiles and targets. The response functions and the light output yields have been measured and compared with the calculations. Disagreements between experiment and calculation have been noted for neutron energy beyond 200 MeV.

2. Experiment

2.1. Experimental setup

The measurements were carried out using the HIMAC heavy-ion synchrotron. Fig. 1 shows the experimental setup at the HIMAC. The NE213 scintillator was placed 5 m downstream of the target at 15(400 MeV/nucleon C ion beam) and 30° (800 MeV/nucleon Si ion beam) to the beam line to decrease the contribution of the charged particles via fragmentation which is the largest at 0° degree, although high energy neutron yields are the largest at 0° degree.

The combinations of 800 MeV/nucleon Si ions and 400 MeV/nucleon C ions as projectiles, and a carbon target were selected on account of the high production yield of high energy neutrons. A thin NE102A plastic scintillator (30 mm diam. by 0.5 mm thick) coupled with the H3178 photomultiplier and base (Hamamatsu Photonics. Co. Ltd.) was placed just behind the end window (made of 0.1 mm-thick aluminum) of the beam line as a beam pick-up scintillator. The output pulses of this scintillator were used as start signals for the neutron time-of-flight (TOF) measurement. These output pulses were also used to count the absolute number of projectiles incident to the target. To avoid the counting loss due to the voltage drop of the photomultiplier, which was induced by high beam current, the voltages of the last three dynodes were externally supplied by a constant-voltage power supply. The carbon target (10 cm by 10 cm square and 23 cm long for Si ion, 20 cm long for C ion) to stop an incident beam

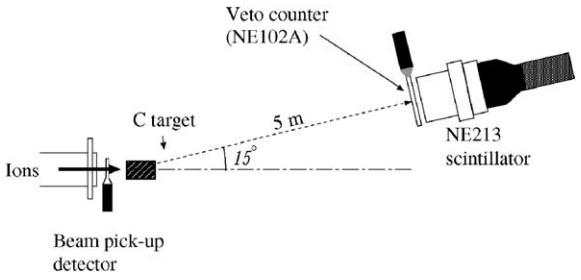

Fig. 1. Experimental setup at the HIMAC.

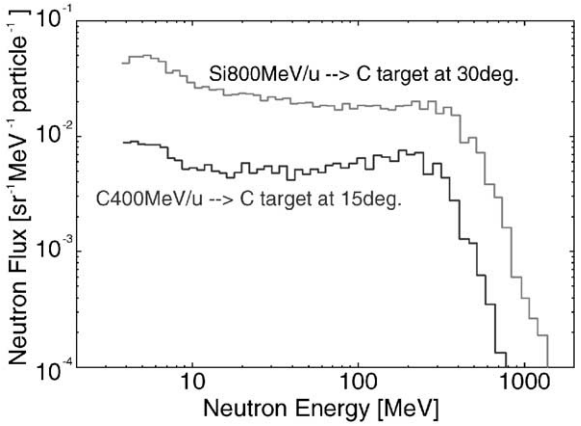

Fig. 2. Source neutron spectra generated from thick carbon target bombarding by 800 MeV/nucleon Si [19] and 400 MeV/nucleon C beams [18].

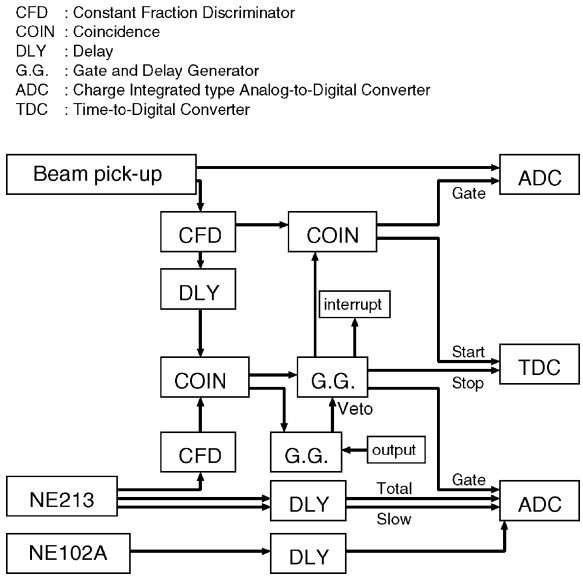

Fig. 3. Schematic diagram for data taking.

completely was set on the beam line 10 cm behind the beam pick-up scintillator.

The energy of a neutron produced in the target was measured by the TOF method. The NE213 scintillator (12.7 cm diam. by 12.7 cm thick) was coupled with the R4144 photomultiplier connected to E1458 base (Hamamatsu Photonics. Co. Ltd.), which is designed to expand the dynamic range of output pulses for high-energy neutron measurements [4]. The NE102A plastic scintillator (15 cm by 15 cm square and 0.5 cm thick), coupled with the H1949 photomultiplier and base (Hamamatsu Photonics. Co. Ltd.), was placed in front of the NE213 scintillator as a veto counter to discriminate charged particles from non-charged particles, neutrons and photons. The source neutron spectra used in the experiments are shown in Fig. 2 cited from Refs. [18] and [19], where the CECIL code has been used to obtain the absolute neutron yields.

2.2. Measuring circuit

A schematic diagram of the experimental arrangement to collect data is presented in Fig. 3. The signal from the beam pick-up scintillator was divided into two pulses, and one pulse was fed to a constant fraction discriminator (CFD) to start a 2048-channel CAMAC time-to-digital converter (TDC) and to count the number of incident beam particles. The other pulse was fed to a charge-integrated type 2249A analog to digital converter (ADC) to obtain pulse height data. The gate pulse of the 2249A was generated by the CFD output of the beam pick-up scintillator. The anode signal from the NE213 scintillator was split into three pulses. One signal was fed to a CFD to produce the stop signal for the TDC and the gate of the ADC. The other two signals were sent through different delay cables to two ADC channels to measure the total and slow light components. The total gate width is 200 ns long during which the whole component of the signal is integrated, and the slow gate starts from 15 ns delayed from the peak of output signal and the width is also 200 ns. The gate timing of the total and slow light components is given in Ref. [18]. The anode signal from each veto counter was also fed to the ADC to get pulse-height data. It is necessary to inhibit the gate pulse of the ADC and the start pulse of the TDC while the computer is busy, so a computer-busy pulse, which was started by the CFD logic pulse of the NE213 and stopped by the 16-bit output generated by the computer immediately after the ADC clear, was put into common inhibit

of the coincidence logic to block the gate pulse of ADC. These data from the CAMAC system were recorded in an event by event mode on a 3.5-inch Magneto-Optical disk by a personal computer using the Kakuken On-line Data Acquisition System (KODAQ) [20].

3. Analysis

3.1. Raw data analysis

The charged particles coming from the target can be eliminated by the light output of the veto counter as shown in Fig. 4(a), since only charged particle events have light outputs in the veto counter. The primary ion intensity was controlled to be about 3×10^5 ions/s not only to suppress the dead time, but also to decrease the pile-up components. The events caused by single particle incidence are selected using the light output of the beam pick-up scintillator as shown in Fig. 4(b). As clearly shown in this figure, when two or three projectiles pass through the beam pick-up scintillator coincidentally, the pulse heights appear two or three times higher than that of a single projectile. The ratio of events caused by a single projectile to all the events is employed to correct the number of projectiles which determine the neutron fluence. This ratio was kept above 90%, and the dead time was about 20% during the experiment.

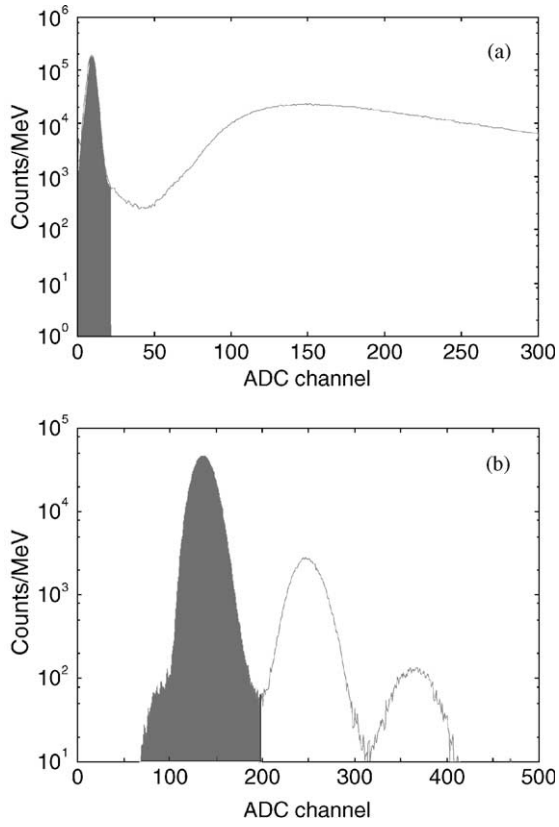

Fig. 4. Light output spectra of (a) the veto counter and (b) the beam pick-up detector. The regions of interest (ROI) are the shaded area.

The neutron and γ-ray events are usually separated by using two-dimensional graphical plots of slow and total component pulse-heights (Fig. 5). When charged particles produced by neutron reactions (mainly recoil protons by the H(n,n)p elastic collision) escape from the NE213 scintillator without complete energy loss, the pulse shapes from high energy neutron events are close to those from γ-ray events, that is called as wall effect, and it is impossible to discriminate only the γ-ray events as shown in Fig. 5. In this study, we removed both events caused by γ-rays and those caused by escaping charged particles. Therefore, the response functions that will be mentioned later exclude the light outputs caused by the escaping charged particles.

The neutron energy incident to the NE213 scintillator can be determined by the time-of-flight spectrum. The neutron energy boundaries were chosen as 50, 60, 70, 80, 100, 120, 140, 160, 180, 220, 260, 320, 400, 550 and 800 MeV considering the neutron yields, variation of the light output spectra and energy resolution of the measuring system.

3.2. Energy calibration

The light output data in channel are converted into the light output unit (MeVee unit). The method of energy calibration commonly used is to measure the γ-rays from standard sources, for example, ^{60}Co, ^{22}Na, ^{241}Am–Be and so on. The threshold of data taking can be changed by the

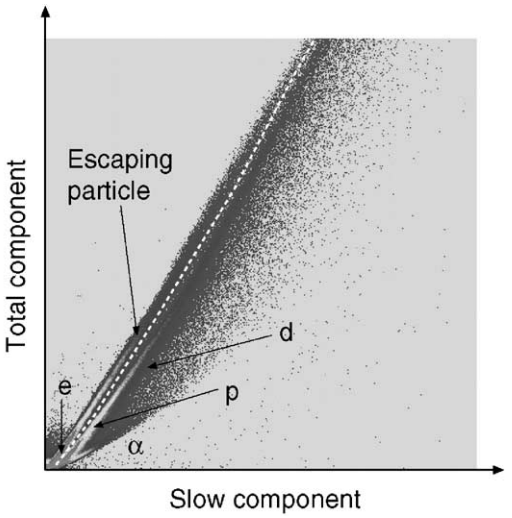

Fig. 5. Two-dimensional scatter plots of the slow component versus total component to identify the particles produced in the NE213 scintillator. The discrimination boundary is indicated by the broken line. The symbol *e* denotes the electron produced by photons and *p*, *d*, α, are for the proton, deuteron and alpha particle produced by neutrons.

dial of the CFD (ORTEC 935). This was set at minimum value for calibration by the standard sources, and was set at about 100 mV (1.5 MeVee) for measurement in order to decrease dead time. As already pointed out in Ref. [4], however, only using the γ-ray sources introduces a large error of the energy calibration for high energy neutron pulses.

In this study, protons generated by the fragmentation reaction are very helpful to calibrate the light output channel into MeVee unit. Although the standard sources are used for calibration, this method was also applied to determine the calibration parameters. Fig. 6 shows the two-dimensional graphical plots of time-of-flight versus total component pulse-heights; the left side figure, (a), gives the raw data of the light outputs in the NE213 from incident non-charged and charged particles, and the right side one, (b), is after elimination of the fragment particles with the coincidence technique of the veto counter pulses to non-charged (neutrons and photons) particles (the hatched area of Fig. 4(a)). Among the fragment particles of protons, deuterons, tritons, ^{3}He and α-particles, protons occupy a dominant fraction and can easily be identified.

The energy of a proton is determined by the time-of-flight with the relativistic kinematics as well as that of a neutron. The proton energy obtained is just the proton energy before it penetrates the veto counter. By taking into account the energy losses [21] in the veto counter and the aluminum window (1.5 mm thick) of the NE213 scintillator, the actual proton energy

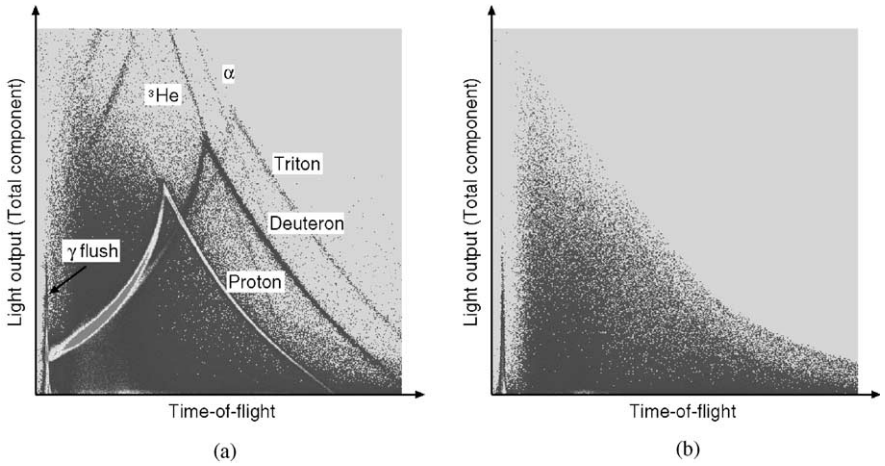

Fig. 6. The two-dimensional graphical plots of time-of-flight versus total pulse-height. The left side figure (a), gives the raw data and the right side one (b), is after eliminating the incident charged particles.

contributed to the scintillation phenomenon can be obtained. Some proton light outputs in the energy range from 40 to 100 MeV were selected to be used for the calibration using the following expression [4]:

$$L = a_1 E_p - a_2\{1.0 - \exp(-a_3 E_p)\},$$

where, L is light output in MeVee unit, E_p is the actual proton energy and factors of a_1, a_2 and a_3 are 0.81, 2.8, 0.20, respectively [4]. By the least square fitting between the channels and light outputs with the obtained data and γ-ray sources, ADC channel data can be converted into MeVee unit.

3.3. Resolution and uncertainties

For measurement of neutron energies by the TOF method, the relative energy resolution is given by the expressions

$$\frac{\Delta E_t}{E} = \gamma(\gamma+1)\left(\frac{\Delta t}{t}\right), \quad \gamma = 1 + \frac{E}{mc^2}$$

where E is the neutron kinetic energy, m the neutron rest mass, Δt the overall time resolution, and t the neutron flight time. The values of $\Delta E_t/E$ have already been estimated in Ref. [17]. In the case of 5 m flight path used in this experiment, the neutron energy resolution gradually increases with neutron energy; 6.9% at 50 MeV, 8.7% at 100 MeV, 11.0% at 200 MeV and 13.5% at 400 MeV.

By repeating the measurements, the statistical uncertainties of the number of source neutrons incident to the NE213 scintillator are found to be below 3%, and the statistical uncertainties for lower light output yields are also below 3% but increase to about 30% at the highest light output yields for incident neutron energies from 50 to 550 MeV. With regard to the response functions for 550–800 MeV neutrons, the statistical uncertainties of the light yields are about 10–30% in the whole region because of the relatively lower source neutron intensity.

4. Results and discussions

4.1. Response functions

The response functions obtained by the experiment are illustrated in Figs. 7 and 8. The alphabets which appear at the left shoulders of each spectra from "A" to "O" correspond to the neutron energy boundaries listed in the figures. Although the threshold of the measurement was 1.5 MeVee as mentioned before, the principal interest of this study is the distribution of higher light output yields so that the curves of the response functions are all presented above 10 MeVee threshold.

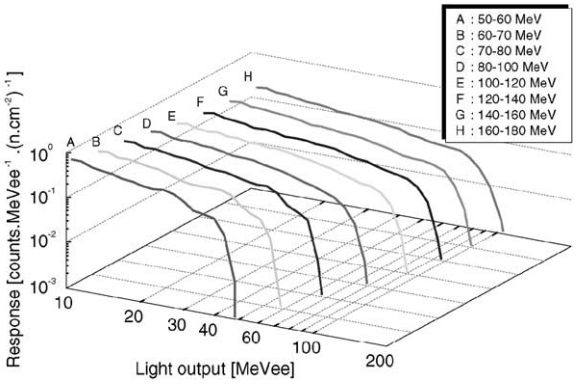

Fig. 7. Measured response functions of the NE213 scintillator for 50–60, 60–70, 70–80, 80–100, 100–120, 120–140, 140–160 and 160–180 MeV neutrons, respectively.

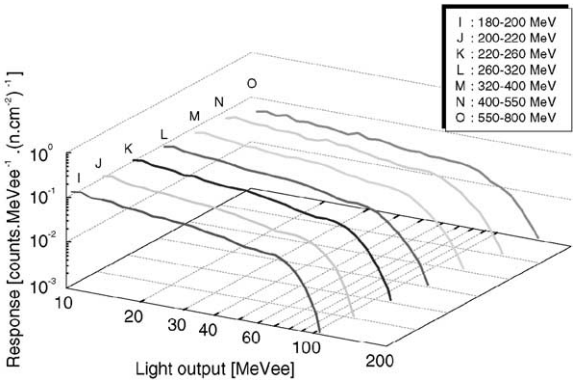

Fig. 8. Measured response functions of the NE213 scintillator for 180–200, 200–220, 220–260, 260–320, 320–400, 400–550 and 550–800 MeV neutrons, respectively.

In the curve "A", the peak of deuterons via C(n, d) reaction around 25 MeVee can be seen. This peak can also be seen on the curves "B" at 36 MeVee and "C" at 40 MeVee, but after the curve "D", the peak cannot be clearly seen since the C(n, d) cross-section gradually decreases while the C(n, np) cross-section increases. The light output distribution caused by the C(n, np) reaction does not indicate the peak as clearly as that caused by the C(n, d) reaction. At the 10 MeVee light outputs of each response, the yields gradually decrease on increasing the neutron energy. This is because the neutron-induced charged particle components escaping from the NE213 scintillator are excluded in the analysis as mentioned before.

It has been hitherto said that the response function does not change above a few hundred MeV region where the charged particles produced by neutron reactions escape from the scintillator, and indeed, the whole shape and the upper edge of the response functions are very similar to each other beyond 200 MeV neutrons. But as shown in the graphs obtained by this experiment, a small change of the response function and a further expansion of the upper edge to higher light output can be clearly seen up to 800 MeV by choosing a wide neutron energy interval beyond 200 MeV. The event which induces such large light output might be caused by the multiple collisions through the C(n, x) reaction in the NE213 scintillator, and the resultant charged particles, such as Be, Li and α particle, which have higher energy transfer from the incident neutron with increasing neutron energy. This can be estimated from the two dimensional plots of time-of-flight pulses versus total component light outputs illustrated in Fig. 6(a). In Fig. 6(a), the maximum values of light outputs from proton, deuteron, triton, ^{3}He and α particles become larger in this order. To clarify the detailed mechanism of light yield, very complicated C(n, x) reaction and its contribution to light outputs must be investigated.

The measured response functions to 130–135, 205–210 and 400–550 MeV neutrons are compared with the results calculated by the CECIL code [7] in Fig. 9. In the cases of 130–135 and 205–210 MeV neutrons, our experimental results are also compared with the experimental results

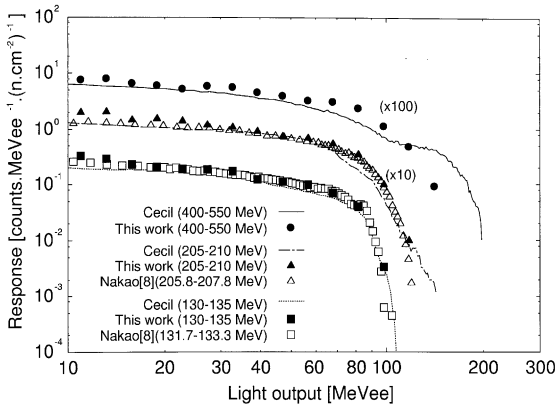

Fig. 9. Measured response functions of the NE213 scintillator for 400–550, 205–210 and 130–135 MeV neutrons compared with the CECIL calculation [7] and Nakao's data [8].

obtained by Nakao [8]. The contribution to light output from the charged particles escaping from the detector is excluded in the CECIL calculation. For 130–135 MeV and 205–210 neutrons, the response functions obtained by this work are in good agreement in absolute values with Nakao's data and the CECIL calculations although a slight disagreement can be seen in the low light output region. For 400–450 MeV neutrons, a large discrepancy in the upper energy region can be seen. The difference in upper light outputs between our data and the CECIL calculation gradually increases with the neutron energy. As already pointed out [8], this discrepancy is introduced by the inaccurate light output approximation used in the CECIL code.

4.2. Tendency of light output

This different increasing tendency of the light output with the incident neutron energies clearly observed by comparison of the light output having the response value of 10^{-3} (counts/MeVee/(n/cm)) between the experiment and the CECIL calculation is shown in Fig. 10. The light outputs which were experimentally obtained monotonously increase with the neutron energy while some fluctuation can be observed in the CECIL calculations. Both light outputs are in good agreement below 100 MeV, but the CECIL results indicate an overestimation from 100 to

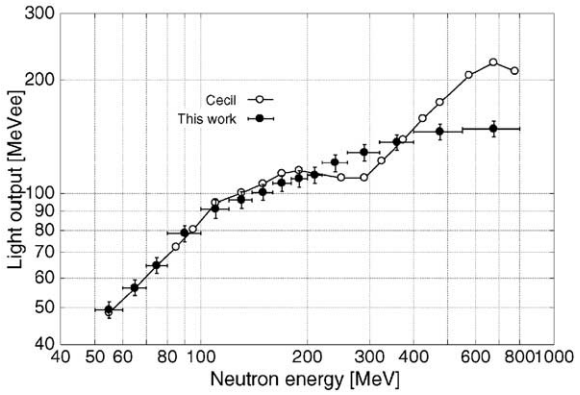

Fig. 10. Comparison of the increasing tendency of the light output having the response value of 10^{-3} (counts/MeVee/(n/cm)) for each incident neutron energy between the experiment and the CECIL calculation.

200 MeV, an underestimation from 200 to 350 MeV and a large overestimation above 350 MeV. These discrepancies are introduced by the hypothesis of reaction cross-sections being kept constant above 200 MeV. The CECIL code treats insufficient number of reaction channels and considers the light output only for protons and α particles. Therefore, it is not capable of simulating the pion production processes: e.g. $np \rightarrow d\pi^0$ and $np \rightarrow d\pi^- \pi^+$.

As a result, measurement of the neutron energy spectrum over 200 MeV by the unfolding method could be done by using the obtained response functions up to 800 MeV although the energy resolution becomes poor.

5. Conclusions

The neutron response functions of 12.7 cm diameter by 12.7 cm long NE213 organic liquid scintillator up to 800 MeV neutrons were measured at the HIMAC . A slight variation of the response functions could be observed with increasing neutron energy, which clarified that the neutron spectrum up to 800 MeV can be obtained by using this scintillator, although the energy resolution becomes poor with the neutron energy. This result is also useful to investigate the light output mechanism in the scintillator for the better Monte Carlo simulation.

Acknowledgements

The authors are deeply grateful to the accelerator operation staffs at HIMAC for their kind cooperation during the experiments. This work has been done as a Research Project with Heavy Ions at NIRS-HIMAC.

References

[1] J.A. Lockwood, C. Chen, L.A. Friling, D. Swartz, R.N.St. Onge, A. Galonsky, R.R. Doering, Nucl. Instr. and Meth. 138 (1976) 353.
[2] Y. Uwamino, K. Shin, M. Fujii, T. Nakamura, Nucl. Instr. and Meth. 204 (1982) 179.
[3] K. Shin, Y. Ishii, Y. Uwamino, H. Sakai, S. Numata, Nucl. Instr. and Meth. A 308 (1991) 609.
[4] N. Nakao, T. Nakamura, M. Baba, Y. Uwamino, N. Nakanishi, H. Nakashima, S. Tanaka, Nucl. Instr. and Meth. A 362 (1995) 454.
[5] R.E. Textor, V.V. Verbinski, ORNL-4160, Oak Ridge National Laboratory, 1968.
[6] J.K. Dickens, ORNL-6463, Oak Ridge National Laboratory, 1988.
[7] R.A. Cecil, B.D. Anderson, R. Madey, Nucl. Instr. and Meth. 161 (1979) 439.
[8] N. Nakao, T. Kurosawa, T. Nakamura, Y. Uwamino, Nucl. Instr. and Meth. A 463 (2001) 275.
[9] N. Nakao, Y. Uwamino, T. Nakamura, T. Shibata, N. Nakanishi, M. Takada, E. Kim, T. Kurosawa, Nucl. Instr. and Meth. A 420 (1999) 218.
[10] W.C. Sailor, R.C. Byrd, Y. Yariv, Nucl. Instr. and Meth. A 277 (1989) 599.
[11] F. Borne, et al., Nucl. Instr. and Meth. A 385 (1997) 339.
[12] W.R. Burrus, V.V. Verbinski, Nucl. Instr. and Meth. 67 (1969) 181.
[13] K. Shin, et al., Nucl. Technol. 53 (1981) 78.
[14] R.H. Johnson, B.W. Wehring, ORNL/RSIC-40, Oak Ridge National Laboratory, 1976.
[15] T. Nakamura, Indian J. Phys. Part A 58A (1984) 12.
[16] N. Nakao et al., Proceedings of the 1993 Symposium on Nuclear Data (JAERI-M 94-019), 1994, p. 183.
[17] T. Kurosawa, N. Nakao, T. Nakamura, Y. Uwamino, T. Shibata, A. Fukumura, K. Murakami, J. Nucl. Sci. Technol. 36 (1999) 41.
[18] T. Kurosawa, N. Nakao, T. Nakamura, Y. Uwamino, T. Shibata, A. Fukumura, K. Murakami, Nucl. Sci. Eng. 132 (1999) 30.
[19] T. Kurosawa, et al., Phys. Rev. C 62 (2000) 044615.
[20] K. Omata, INS Report INS-T-496, 1990.
[21] T.W. Armstrong, ORNL-4869 Oak Ridge National Laboratory, 1973.